High operating temperature mid-infrared InGaAs/GaAs submonolayer quantum dot quantum cascade detectors on silicon

Daqian Guo, Jian Huang, Mourad Benamara, Yuriy I. Mazur, Zhuo Deng, Gregory J. Salamo, Huiyun Liu, Baile Chen, Jiang Wu

***Abstract*—Monolithic integration of infrared photodetectors on a silicon platform is a promising solution for the development of scalable and affordable photodetectors and infrared focal plane arrays. We report on integration of submonolayer quantum dot quantum cascade detectors (SML QD QCDs) on Si substrates via direct growth. Threading dislocation density has been reduced to the level of $\sim 10^7$ cm^{-2} with the high-quality GaAs-on-Si virtual substrate. We also conducted a morphology analysis for the SML QD QCDs through a transmission electron microscope strain contrast image and to the best of our knowledge, high quality InGaAs/GaAs SML QDs were clearly observed on silicon for the first time. Photoluminescence decay time of the as-grown SML QD QCDs on Si was measured to be around 300 ps, which is comparable to the reference QCDs on lattice-matched GaAs substrates. With the high-quality III-V epitaxial layers and SML QDs, the quantum cascade detectors on Si achieved a normal incident photoresponse temperature up to 160 K under zero bias.**

***Index Terms*—submonolayer quantum dots, quantum cascade detectors, silicon, molecular beam epitaxy**

I. Introduction

THERE is a momentum to use the well-established group IV wafers as alternative epitaxial substrates to grow III-V optoelectronic devices, e.g., lasers, infrared photodetectors and so on [1–7]. High-quality and large-area Si substrates are widely accessible and compared with the III-V counterparts, have the advantages in price, size, mechanical strength, and a matched thermal expansion coefficient with Si based readout circuitry [8]. Monolithic integration of III-V infrared detectors via direct growth enables cost-effective manufacturing and increased reliability. This would open the possibility of manufacturing III-V detectors along with Si optoelectronic and electronic devices, taking the advantages of mature Si CMOS foundries. Over the past few decades, great effort has been paid to address the difficulties associated with the heteroepitaxy and the progresses have paved a feasible path toward reliable virtual substrates, for example, record low threading dislocation densities (TDDs) have been reported recently by different research groups [9–11].

Quantum cascade detectors (QCDs) have recently gained attentions because they can operate without applying bias in a photovoltaic mode [12]. For the absorption medium of a QCD, either quantum wells (QWs) or quantum dots (QDs) are suited. The QW absorbers are relatively easy to couple with the successive cascade QWs and the intersubband transition energy is well studied. QCDs based on QW absorbers (QW QCDs) have been reported in a wide spectrum ranging from near infrared to very long wavelength infrared [13–16]. QCDs based on QD absorber were first demonstrated by Brave et al. to address the issues that intersubband selection rules prohibit the normal incidence absorption in QWs [17]. The absorber in the work was 5 stacks of InAs/InGaAs/GaAs/AlGaAs QDs-in-a-well with peak response wavelength at about 5.5 μm. Wang et al. reported 20 periods of strain-compensated InAs QD QCDs on InP substrates [18].

In both Brave's and Wang's work, the QDs were grown by the self-assembled Stranski-Krastanov (S-K) method, where a significant fraction of InAs is used to form a 2D wetting layer prior to the onset of 3D InAs QDs. The wetting layer does not contribute to the normal incidence absorption, whereas the strain can build up. Submonolayer (SML) QD is an attractive alternative to the S-K QD offering several advantages including absence of wetting layers and high areal density. The SML QDs can be grown by altering depositions of InAs material with a nominal thickness less than one ML and a few MLs of GaAs spacer. The deposited InAs materials tend to form a vertical connected and lateral segregated InAs-rich agglomerations or InAs SML QDs [19]. Since all the deposited InAs materials can participate the formation of SML QDs, the amount of lattice mismatched materials is reduced. We demonstrated 20 periods of SML QD based QCDs on GaAs and Si substrates with peak response wavelength at about 6 μm [20, 21]. Later, Shen et al. shown the heteroepitaxial grown long-wavelength SML QD QCDs on a Ge substrate [22].

However, previous SML QD QCD work were focusing on device characterizations. Little attention has paid to the structural properties of SML QDs, which is critical for further

The authors would like to acknowledge the support of the National Natural Science Foundation of China under Grant 61974014, the Innovation Group Project of Sichuan Province under Grant 20CXTD0090, and Double First-Class Initiative Fund of ShanghaiTech University. We are grateful to the device fabrication support from the ShanghaiTech University Quantum Device Lab. Corresponding Authors: Baile Chen (chenbl@shanghaitech.edu.cn) and Jiang Wu (jiangwu@uestc.edu.cn).

D. Guo and J. Wu are with Institute of Fundamental and Frontier Sciences, University of Electronic Science and Technology of China, Chengdu 610054, China

J. Huang, Z. Deng, and B. Chen are with Optoelectronic Devices Laboratory, School of Information Science and Technology, ShanghaiTech University, Shanghai 201210, China

M. Benamara, Y. I. Mazur and G.J. Salamo are with Institute for Nanoscience and Engineering, University of Arkansas, Fayetteville, Arkansas 72701, USA

H. Liu is with Department of Electronic and Electrical Engineering, University College London, London WC1E 7JE, United Kingdom

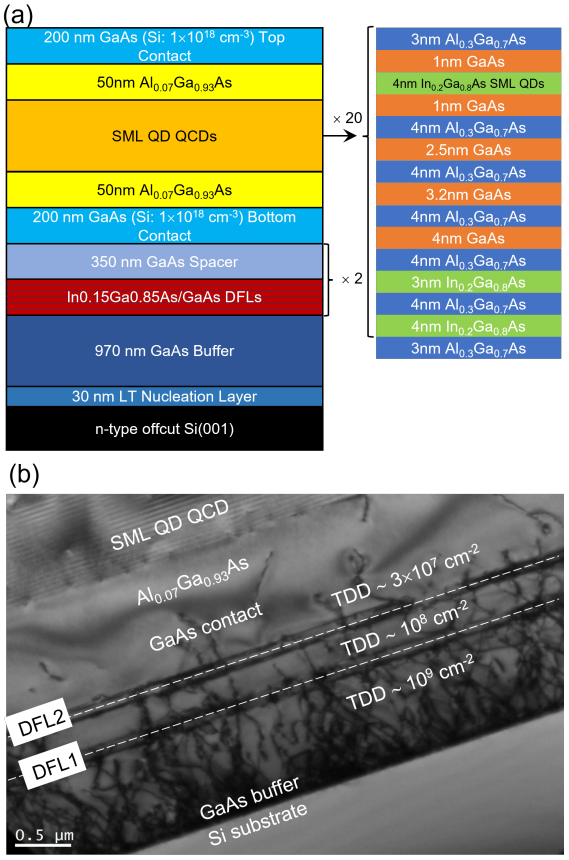

Fig. 1. (a) Structure of SML QD QCD on Si substrates. (b) Bright field (g=220) cross-sectional TEM image of the GaAs-on-Si virtual substrate.

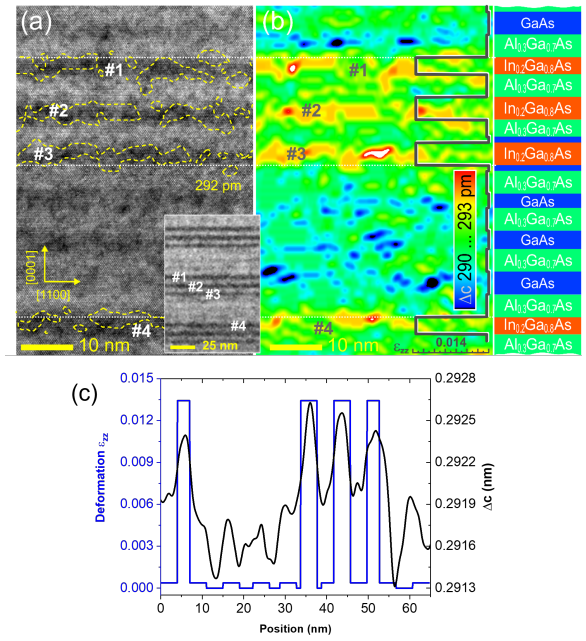

Fig. 2. XTEM images collected along the [110] direction, (a) the GaAs/AlGaAs/InGaAs MQWs structure with several MQW periods shown in the inset. (b) shows a corresponding map of the change in the relaxed lattice constant, Δc, taken from the fringes in the XTEM image with an overlay on the right side showing the simulated, ε_{zz} deformation profile. The dashed lines in (a) show the 292 pm constants spacing underlining the border of the clusters. The numbers 1-4 denote $In_{0.2}Ga_{0.8}As$ layers of the structure shown on the right. (c) simulated deformation profile along the growth direction in the GaAs/AlGaAs/InGaAs MQW structure and the corresponding measured profile of change in the relaxed lattice constant in (b) integrated over a 20 nm width.

optimization of the device performance. In this paper, we extended our studies on the structural characterization of the SML QD QCDs on Si with high resolution cross-sectional transmission electron microscope (HR-XTEM) and photoluminescence (PL) measurements. The TEM strain contrast map reveals the localized InAs agglomerations and outlines the shapes of the SML QD QCDs. PL measurements indicates that the SML QD QCD material on Si has a similar quality to the SML QD QCDs on GaAs in terms of carrier lifetime. Given the high-quality III-V buffer and SML QDs, high operating temperature quantum cascade detectors was achieved on Si up to 160 K under zero bias.

II. Material Growth and Detector Fabrication

The detectors were grown by a solid-source Veeco Gen-930 molecular beam epitaxy system. The overall structure of SML QD QCD on Si has been given in Fig.1 (a). A Si(001) substrate with 4° offcut towards the [011] direction was used for growing the SML QD QCD material on Si. Prior to the growth, the substrate was deoxidized at 900°C for 30 mins. The Si substrate was then transferred to the growth chamber for growing a 5 nm AlAs and a 25 nm GaAs nucleation layers by migration-enhanced epitaxy at 370°C. After the nucleation layer, a 970 nm of GaAs buffer was deposited at 670°C. Two sets of dislocation filter layers (DFL) were grown on top of the GaAs buffer. Each DFL contained ten periods of 10 nm $In_{0.15}Ga_{0.85}As$/10 nm GaAs strained layer superlattices (SLSs) and a 350 nm thick GaAs spacer. TEM revealed that the TDD has been reduced from $\sim 10^9$ to 3×10^7 cm^{-2} with the insertion of two DFLs, Fig.1 (b). On top of the GaAs buffer, the growth of device region was carried out as follow: a 200 nm Si-doped (1×10^{18} cm^{-3}) GaAs bottom contact, a 50 nm $Al_{0.7}Ga_{0.93}As$ barrier, 20 iterations of SML QD QCDs, a 50 nm $Al_{0.7}Ga_{0.93}As$ barrier, and a 200 nm Si-doped (1×10^{18} cm^{-3}) GaAs top contact. Each iteration of the SML QD QCD was grown in the following manner: 3 nm $Al_{0.3}Ga_{0.7}As$, 4 nm $In_{0.2}Ga_{0.8}As$, 4 nm $Al_{0.3}Ga_{0.7}As$, 3 nm $In_{0.2}Ga_{0.8}As$, 4 nm $Al_{0.3}Ga_{0.7}As$, 4nm GaAs, 4 nm $Al_{0.3}Ga_{0.7}As$, 3.2 nm GaAs, 4 nm $Al_{0.3}Ga_{0.7}As$, 2.5 nm GaAs, 4 nm $Al_{0.3}Ga_{0.7}As$, 1 nm GaAs, 4 nm SML QDs and 1 nm GaAs. The SML QD (Si-doped, 1×10^{17} cm^{-3}) region, which has a nominal composition equivalent to $In_{0.2}Ga_{0.8}As$, consists of five stacks of alternating deposited 0.57 ML InAs and 2.26 MLs GaAs. For comparison, a same SML QD QCD structure has been grown on a GaAs substrate.

After the material growth, the materials were fabricated into circular mesa detector structure by standard photolithography and wet chemical etching. The QCDs were fabricated into circular mesa structures by photolithography and wet chemical etching. Diameter of the detectors under test were 210 μm. Ni/AuGe/Ni/Au metallic films were deposited at the top and bottom GaAs contacts and followed by a rapid thermal

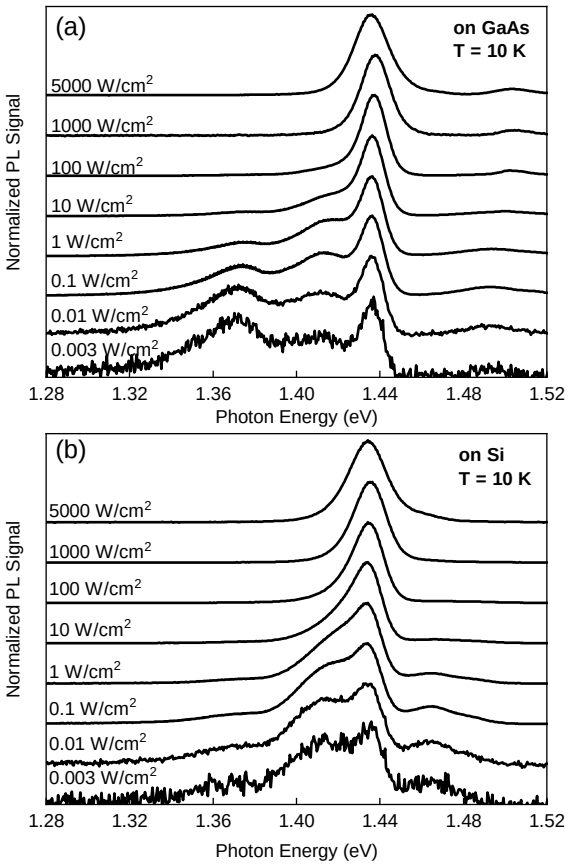

Fig. 3. Low temperature power dependent PL measurements for the QCDs (a) on GaAs and (b) on Si substrates.

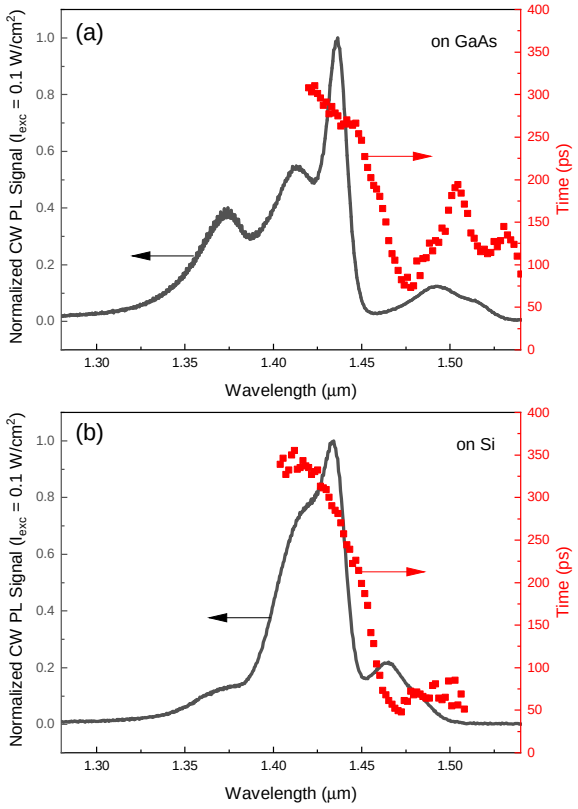

Fig. 4. PL decay lifetime at 10 K for the QCDs on (a) GaAs and on (b) Si substrates.

annealing for ohmic contacts.

III. Material Characterizations

The as-grown SML QDs can be considered as InAs-rich agglomerations buried in the GaAs matrix. The regions with higher In content have larger atomic spacing leading to localized strain and inhomogeneous deformation distributions in both in-plane and growth directions. To have a visualized strain contrast information within the device region, XTEM results were captured for the QCD on Si and shown in Fig. 2. The horizontal dark grey lines in Fig. 2 (a) and the insert correspond to different layers of the GaAs/AlGaAs/InGaAs multiple QWs (MQWs) structure. The captured area was free from threading dislocations. fig. 2 (b) maps the lattice spacing using an image segmentation and Fourier analysis algorithm. The $In_{0.2}Ga_{0.8}As$ layers (#1 to #4) can be easily identified due to their observable increase from the AlGaAs/GaAs background. The deformation, ε_{zz}, through layers of the investigated MQWs structure was simulated using NextNano software and are shown in Fig. 2 (b) and (c). It could be noticed that the SML QDs layer has a higher strain deformation than the other $In_{0.2}Ga_{0.8}As$ layers. The yellow dashed lines representing the 292 pm contour lines were mirrored form the lattice spacing map, which can be used to highlight the In-rich agglomerations. There is no noticeable difference between the SML QD layer and the InGaAs/AlGaAs QW layers in terms of the shape. This indicates that the surface undulations during heteroepitaxy of III-Vs on silicon may also promote In agglomerations in the QW layers which would undermine the carrier transport via the cascade structures. Moreover, the shapes of the InAs clusters in the SML QD layer (#3) are irregular and they favour to elongate in the lateral direction. The laterally elongated SML QDs have no contribution to the normal incident absorption oscillator strength but reduces the dot areal density [23]. Future work should focus on preventing the In agglomerations in the QW layers and in-pane coalesce of the SML QDs and optimize the growth process with larger spacing.

To characterize the optical properties and electronic structure of the SML QD QCDs on Si and GaAs substrates, low temperature power-dependent PL measurements were carried out using a variable power Nd:YAG laser (λ = 532 nm). Fig.3 (a) and (b) present the PL spectra measured under different laser power densities at 10 K. For the detector on GaAs, three primary peaks can be identified at about 1.37, 1.42 and 1.44 eV with full-width-at-half-maximum (FWHM) values of 35, 27 and 10 meV. The two broad peaks on the left attributed to the emissions from the ground states and excited states of the InGaAs clusters [19]. The narrow linewidth peak at 1.44 eV suggested the ground state emission of the MQWs. With increasing excitation power, the peak intensity at ~1.44 eV gradually outcompeted the two low energy peaks and became the major peak for the GaAs sample. For the detector on Si under low laser intensities, the emission peaks had the

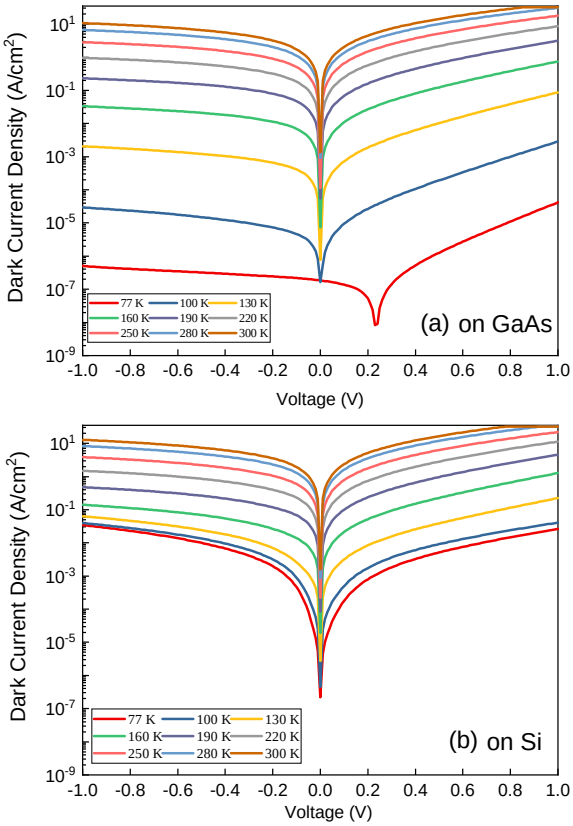

Fig. 5. Dark current density as a function of bias voltage (J-V) for QCDs (a) on GaAs and (b) on Si.

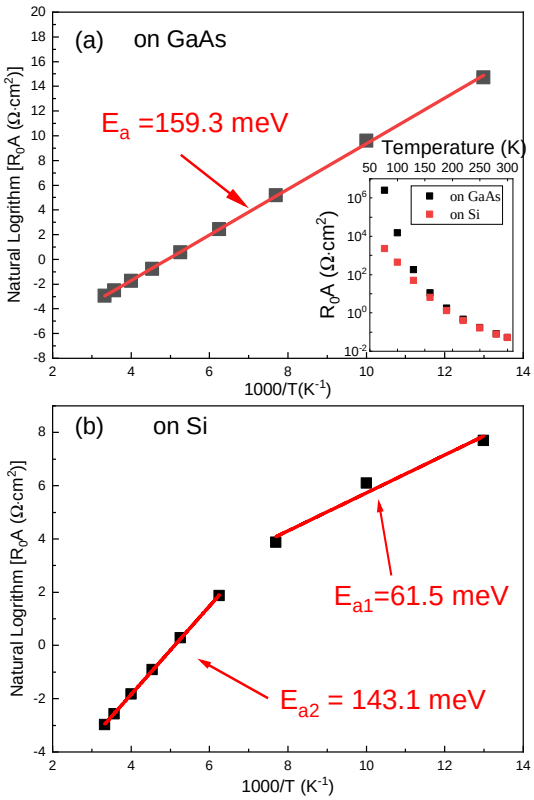

Fig. 6. Arrhenius plots for QCDs on GaAs and on Si, respectively. The insert is the plot of R_0A values and the corresponding temperatures.

same positions as peak positions for the GaAs sample, but with a slightly larger FWHM values of 41, 29 and 12 meV for the peaks at 1.37, 1.42 and 1.44 eV, respectively. To obtain more information on the material quality, time resolved PLs were performed using 2 ps pulses of 720 nm excitation from a mode-locked Ti-sapphire laser that produces an optical pulse train at 76 MHz and a Hamamatsu Synchroscan C5680 streak camera with an infrared enhanced S1 cathode. The laser excitation density per pulse was 6×10^{11} photons/cm^2. Time resolved PL measurements were carried out by using a pulsed laser source (λ = 750 nm). Fig. 4 shows the time resolved PL measurements for the QCDs on GaAs and Si. Within the region of interest, i.e., 1.40 - 1.45 eV, the PL decay lifetimes of the two materials are within the range of 250-350 ps, despite there is high density of defects in the QCD on Si. Interestingly, the Si sample has a longer PL decay time at ~1.41 eV than the GaAs sample, which may be caused by the surface undulation, and thus stronger quantum confinement, of the QCD on Si.

IV. Device Characterizations

The QCDs were placed in a liquid nitrogen cooled probe station for dark current measurements. The positive bias condition is when the positive terminal connected to the top contact. The measured dark current results and calculated zero-bias resistance-area products (R_0A) are presented in Fig. 5 and Fig. 6. For the minimum dark current that not occurred at 0 V, is due to the imperfect shielding. The higher dark current under positive bias is due the asymmetric band profile. At 77 K, the R_0A values are 2.5×10^6 $\Omega\cdot$cm^2 and 2.2×10^3 $\Omega\cdot$cm^2 for the QCD on GaAs and Si, respectively. At 160 K, the R_0A values reduced to 11.32 $\Omega\cdot$cm^2 for the QCD on GaAs and 6.45 $\Omega\cdot$cm^2 for the QCD on Si. To understand the origins of the low R_0A in the QCD on Si, Arrhenius plots have been shown in Fig. 6. The activation energy is about 159 meV in QCD on GaAs corresponding to the transitions from the ground state to the first and second GaAs cascade MQWs. For the Si device, there is a leakage path with a much lower activation energy (~ 61.5 meV) at low temperatures, which is accountable for the low R_0A values. At higher temperatures, the activation energy increased to 143.1 meV.

The photoresponse curves of the two detectors were measured using a Nicolet iS50 Fourier transform spectrometer under normal incidence configuration. A 700 °C blackbody source was used to calibrate the responsivity. Fig. 7 (a) and (b) present the responsivity results measured at 77 K, 120 K and 160 K for the two devices. The two detectors had similar photoresponse curves spanning a broad range of spectrum from 5.5 μm to 7.5 μm at 77 K. Two response peaks could be found for both samples at all measured temperatures. These two response peaks are most likely originated from two intersubband transitions in the SML QD absorber. The highest temperature for a measurable photoresponse curve was obtained at 180 K for the QCDs on GaAs and the QCD on Si has achieved a maximum operating temperature at 160 K. It is worth noting that the maximum operating

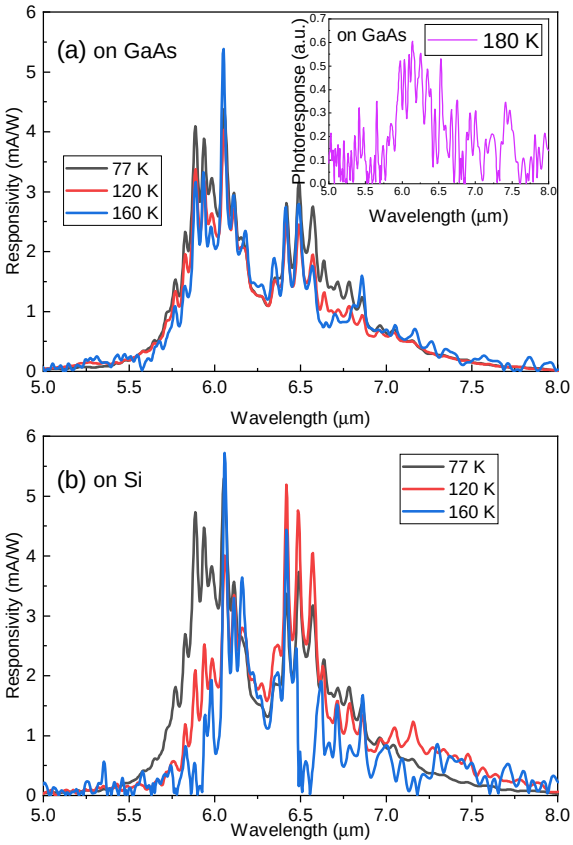

Fig. 7. (a) and (b) are the calibrated photoresponsivities at 77, 120, 160 K for the QCDs on GaAs and Si, respectively. Insert in (a) is measured photoresponse at 180 K for the QCD on GaAs.

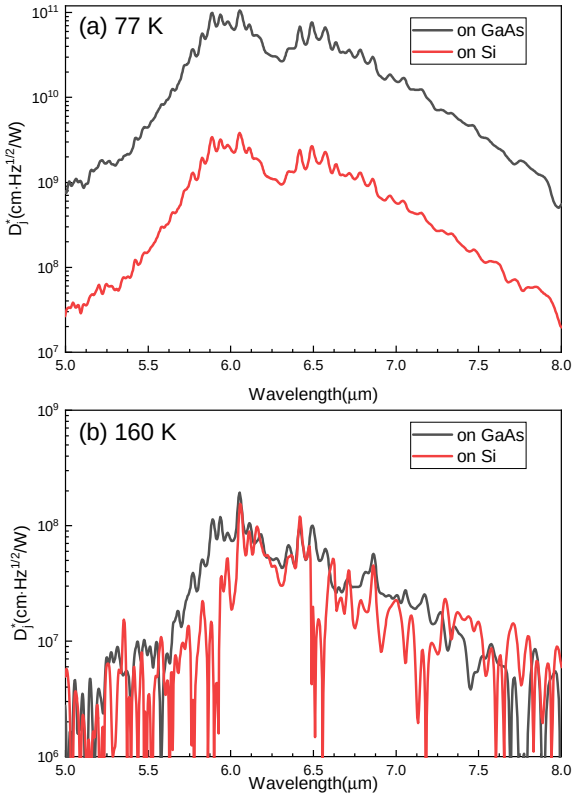

Fig. 8. Johnson noise limited detectivity (D_j^*) curves obtained at (a) 77 K and (b) 160 K for GaAs and Si samples.

temperature above 130 K was not obtained from our previous work [20, 21]. We considered that the improved signal-to-noise ratios at high temperatures was contributed by improved material quality and fabrication. Compared with our previously published photoconductive QD infrared photodetectors on Si [7, 24], where the measured temperatures were lower than 80 K, the designed SML QD QCD on Si has better capabilities for high operating temperature applications. Higher operating temperature and better performance could be expected with optimizations in material quality, particularly the QD and cascade layers, and structural design.

For QCDs operating at zero bias, the main source of dark current is the Johnson noise. The Johnson noise limited detectivity (D_j^*) can be calculated by the following equation,

$$D_j^* = R\sqrt{R_0 A/4k_B T} \tag{1}$$

where R is the responsivity, k_B is the Boltzmann constant and T is the temperature. Fig. 8 shows the calculated Johnson limited detectivities at (a) 77 K and (b) 160 K. The QCD on GaAs has a maximum D_j^* of 1.06×10^{11} cm· $Hz^{1/2}$/W at 77 K, roughly 30 times higher than the QCD on Si (3.83×10^9 cm· $Hz^{1/2}$/W), mainly due to the high R_0A value, i.e., low Johnson noise. At 160 K, the maximum Johnson noise-limited detectivities dropped to 1.98×10^8 cm· $Hz^{1/2}$/W and 1.55×10^8 cm· $Hz^{1/2}$/W for the QCDs on GaAs and Si, respectively.

V. Conclusions

In conclusion, we have presented the material and device characterizations of SML QD QCDs on Si substrates. High quality of GaAs-on-Si virtual buffer has been grown on the Si substrate. With the strain contrast image and lattice spacing mapping, we managed to identify the localized In-rich regions that form the SML QDs. In agglomerations in the QW layers were also observed, which should be avoided in future studies. The low temperature power dependent PL and PL decay lifetime experiments indicate a high-quality material on Si substrates, which is comparable with the material on GaAs. The two detectors have the almost identical photocurrent response at mid-infrared range from 5.5 μm to 7.5 μm at 77 K under normal incident configuration. The high-quality GaAs-on-Si virtual substrates also enables high operating temperature as high as 160 K for the QCDs on Si. The peak Johnson noise-limited detectivities are 1.55×10^8 and 1.98×10^8 cm· $Hz^{1/2}$/W for the QCDs on Si and GaAs, respectively, at 160 K.

References

[1] A. Johnson, A. Joel, A. Clark, D. Pearce, M. Geen, W. Wang, R. Pelzel, and S. Lim, "High performance 940nm VCSELs on large area germanium substrates: the ideal substrate for volume manufacture," in *Vertical-Cavity Surface-Emitting Lasers XXV*. SPIE, 2021.

[2] E. Delli, V. Letka, P. Hodgson, E. Repiso, J. Hayton, A. Craig, Q. Lu, R. Beanland, A. Krier, A. Marshall, and P. Carrington, "Mid-Infrared InAs/InAsSb Superlattice

nBn Photodetector Monolithically Integrated onto Silicon," *ACS Photonics*, vol. 6, no. 2, pp. 538–544, 2019.

[3] Z. Deng, D. Guo, C. Burguete, Z. Xie, J. Huang, H. Liu, J. Wu, and B. Chen, "Demonstration of Si based InAs/GaSb type-II superlattice p-i-n photodetector," *Infrared Physics & Technology*, vol. 101, pp. 133–137, 2019.

[4] Y. Zhang, A. Haddadi, R. Chevallier, A. Dehzangi, and M. Razeghi, "Thin-Film Antimonide-Based Photodetectors Integrated on Si," *IEEE Journal of Quantum Electronics*, vol. 54, no. 2, pp. 1–7, 2018.

[5] Y. Wan, Z. Zhang, R. Chao, J. Norman, D. Jung, C. Shang, Q. Li, M. Kennedy, D. Liang, C. Zhang, J.-W. Shi, A. C. Gossard, K. M. Lau, and J. E. Bowers, "Monolithically integrated InAs/InGaAs quantum dot photodetectors on silicon substrates," *Optics Express*, vol. 25, no. 22, p. 27715, oct 2017.

[6] B. Chen, Y. Wan, Z. Xie, J. Huang, N. Zhang, C. Shang, J. Norman, Q. Li, Y. Tong, K. M. Lau, A. C. Gossard, and J. E. Bowers, "Low Dark Current High Gain InAs Quantum Dot Avalanche Photodiodes Monolithically Grown on Si," *ACS Photonics*, vol. 7, no. 2, pp. 528–533, 2020.

[7] D. Guo, Q. Jiang, M. Tang, S. Chen, Y. Mazur, Y. Maidaniuk, M. Benamara, M. Semtsiv, W. Masselink, G. Salamo, H. Liu, and J. Wu, "Two-colour $In_{0.5}Ga_{0.5}As$ quantum dot infrared photodetectors on silicon," *Semiconductor Science and Technology*, vol. 33, no. 9, p. 094009, 2018.

[8] A. Rogalski, J. Antoszewski, and L. Faraone, "Third-generation infrared photodetector arrays," *Journal of Applied Physics*, vol. 105, no. 9, p. 091101, 2009.

[9] C. Shang, J. Selvidge, E. Hughes, J. C. Norman, A. A. Taylor, A. C. Gossard, K. Mukherjee, and J. E. Bowers, "A Pathway to Thin GaAs Virtual Substrate on On-Axis Si (001) with Ultralow Threading Dislocation Density," *physica status solidi (a)*, vol. 218, no. 3, p. 2000402, 2020.

[10] C. Shang, E. Hughes, Y. Wan, M. Dumont, R. Koscica, J. Selvidge, R. Herrick, A. C. Gossard, K. Mukherjee, and J. E. Bowers, "High-temperature reliable quantum-dot lasers on Si with misfit and threading dislocation filters," *Optica*, vol. 8, no. 5, p. 749, 2021.

[11] J. Yang, K. Li, H. Jia, H. Deng, X. Yu, P. Jurczak, J.-S. Park, S. Pan, W. Li, S. Chen, A. Seeds, M. Tang, and H. Liu, "Low threading dislocation density and antiphase boundary free GaAs epitaxially grown on on-axis Si (001) substrates," *Nanoscale*, vol. 14, no. 46, pp. 17 247–17 253, 2022.

[12] L. Gendron, M. Carras, A. Huynh, V. Ortiz, C. Koeniguer, and V. Berger, "Quantum cascade photodetector," *Applied Physics Letters*, vol. 85, no. 14, pp. 2824–2826, 2004.

[13] A. Vardi, G. Bahir, F. Guillot, C. Bougerol, E. Monroy, S. Schacham, M. Tchernycheva, and F. Julien, "Near infrared quantum cascade detector in GaN/AlGaN/AlN heterostructures," *Applied Physics Letters*, vol. 92, no. 1, p. 011112, 2008.

[14] P. Reininger, T. Zederbauer, B. Schwarz, H. Detz, D. Macfarland, A. Andrews, W. Schrenk, and G. Strasser, "InAs/AlAsSb based quantum cascade detector," *Applied Physics Letters*, vol. 107, no. 8, p. 081107, 2015.

[15] N. Kong, J.-Q. Liu, L. Li, F.-Q. Liu, L.-J. Wang, Z.-G. Wang, and W. Lu, "A 10.7 μm InGaAs/InAlAs Quantum Cascade Detector," *Chinese Physics Letters*, vol. 27, no. 12, p. 128503, 2010.

[16] A. Buffaz, M. Carras, L. Doyennette, A. Nedelcu, X. Marcadet, and V. Berger, "Quantum cascade detectors for very long wave infrared detection," *Applied Physics Letters*, vol. 96, no. 17, p. 172101, 2010.

[17] A. Barve and S. Krishna, "Photovoltaic quantum dot quantum cascade infrared photodetector," *Applied Physics Letters*, vol. 100, no. 2, p. 021105, 2012.

[18] X.-J. Wang, S.-Q. Zhai, N. Zhuo, J.-Q. Liu, F.-Q. Liu, S.-M. Liu, and Z.-G. Wang, "Quantum dot quantum cascade infrared photodetector," *Applied Physics Letters*, vol. 104, no. 17, p. 171108, 2014.

[19] A. Lenz, H. Eisele, J. Becker, J.-H. Schulze, T. Germann, F. Luckert, K. Pötschke, E. Lenz, L. Ivanova, A. Strittmatter, D. Bimberg, U. Pohl, and M. Dähne, "Atomic structure and optical properties of InAs submonolayer depositions in GaAs," *Journal of Vacuum Science & Technology B, Nanotechnology and Microelectronics: Materials, Processing, Measurement, and Phenomena*, vol. 29, no. 4, p. 04D104, 2011.

[20] J. Huang, D. Guo, W. Chen, Z. Deng, Y. Bai, T. Wu, Y. Chen, H. Liu, J. Wu, and B. Chen, "Sub-monolayer quantum dot quantum cascade mid-infrared photodetector," *Applied Physics Letters*, vol. 111, no. 25, p. 251104, 2017.

[21] J. Huang, D. Guo, Z. Deng, W. Chen, H. Liu, J. Wu, and B. Chen, "Midwave Infrared Quantum Dot Quantum Cascade Photodetector Monolithically Grown on Silicon Substrate," *Journal of Lightwave Technology*, vol. 36, no. 18, pp. 4033–4038, 2018.

[22] Z. Shen, Z. Deng, X. Zhao, J. Huang, C. Cao, X. Zou, F. Liu, Q. Gong, and B. Chen, "Submonolayer quantum dot quantum cascade long-wave infrared photodetector grown on Ge substrate," *Applied Physics Letters*, vol. 118, no. 8, p. 081102, 2021.

[23] N. Ting, S. Bandara, S. Gunapala, J. Mumolo, S. Keo, C. Hill, J. Liu, E. Blazejewski, S. Rafol, and Y.-C. Chang, "Submonolayer quantum dot infrared photodetector," *Applied Physics Letters*, vol. 94, no. 11, p. 111107, 2009.

[24] J. Wu, Q. Jiang, S. Chen, M. Tang, Y. I. Mazur, Y. Maidaniuk, M. Benamara, M. P. Semtsiv, W. T. Masselink, K. A. Sablon, G. J. Salamo, and H. Liu, "Monolithically Integrated InAs/GaAs Quantum Dot Mid-Infrared Photodetectors on Silicon Substrates," *ACS Photonics*, vol. 3, no. 5, pp. 749–753, 2016.